Analysis of photonic crystal fibers using full vectorial finite difference method

تحليل الألياف البللورية الضوئية باستخدام طريقة الفروق المحددة ذات الوصف الاتجاهي التام

M.Farhat[1*], S.S.A.Obayya [2] and A.M.Nasr[1]**

[1] Department of Mathematical and Physical Sciences, Faculty of Engineering, University of Mansoura, Egypt.
Email: *engmfarhat@mans.edu.eg
** fldp7@mans.edu.eg

[2] Department of Electronics and Communications, Faculty of Engineering, University of Mansoura, Egypt

الملخص العربي:

في هذا البحث تم تطبيق طريقة الفروق المحددة ذات الوصف الاتجاهي التام (FV-FDM)لإيجاد حل لأنماط الانتشار خلال ألياف البللورات الضوئية (PCFs) وتم دراسة تأثير الشكل الهندسي لألياف البللورات الضوئية ذو الفجوات ذات الشكل الدائري أو القطع الناقص على كل من معاملات الانكسار والتشتت وكذلك على المساحة الفعالة لهيئة الانتشار. وقد أعطى الشكل المقترح نتائج للتشتت للنمط الأساسي للانتشار قيمة 0 ±1.288 ps/nm.km في المدى الترددي 1.3ميكرو متر إلى 1.8 ميكرو متر. وتم مناقشة استخدام الشكل المقترح لمثل هذه الألياف كمستشعر للضغط.

Abstract

The full-vectorial finite difference method (FV-FDM) is applied to perform modal solution to photonic crystal fibers (PCFs). The effects of geometrical parameters of the circular and elliptical holes on the effective index, the dispersion and the effective mode area of the fundamental mode have been studied. PCF structure showing dispersion of 0±1.288 ps/nm.km over the wavelength range from 1.3 μm to 1.8 μm has been reported. The applicability of using PCF as a pressure sensor has been discussed.

Keywords: Photonic crystal fiber; Finite difference method; Full-vectorial modes

Accepted May 29, 2007

1- Introduction

Photonic Crystal Fibers (PCFs) [1,2] have been the subject of extensive research in recent years. This due to their unusual and very attractive optical properties such as a wide single mode wavelength range [3], large effective mode area [4] and anomalous dispersion at visible and near infrared wavelengths [5]. They are usually made of silica with a regular array of air holes running along the length of the fiber acting as a cladding. Such structure creates bandgaps where propagation at certain optical frequencies is forbidden. A defect is introduced in the periodic structure in the form of either larger air hole (low index core), or missing hole (high index core) which introduces guided modes within the previously forbidden bandgap.

Intensive research has been ongoing during the last years to develop accurate modeling methods for photonic crystal. Various methods have been developed for modal calculation of such waveguides such as finite difference time domain [6], finite difference method [7] and the finite element method [8, 9]. Due to the simplicity of its implementation and the sparsity of its resultant matrix, mode solvers based on the FDM have become attractive numerical methods for analyzing the propagation characteristics of the optical or dielectric waveguides, especially for those complex dielectric waveguides without analytical solutions. The FDM was first employed to solve the scalar waveguide modes under the weakly guiding approximation [10]. For strongly guiding structures, semi-vectorial equations for optical waveguides with arbitrary index profiles were derived [11, 12]. To obtain more accurate mode fields, a full-vectorial finite difference scheme was then proposed [13–15].

In this paper, the full vectorial mode calculation using finite-difference method (FV-FDM) [15] is used to perform modal analysis of PCFs. The effects of geometrical parameters of the circular and elliptical holes of the PCF on the effective index, the effective mode area and the dispersion of the fundamental mode have been studied thoroughly. PCFs with circular and elliptical holes with low index circular and elliptical core have been also studied. Possibility of using PCFs in

pressure sensing has been discussed. Following this introduction, a brief mathematical analysis of the FV-FDM is introduced in section 2. The validation and simulation results of the modal analysis program are detailed in section 3 by addressing a standard rib waveguide and different PCFs structures. Finally, conclusions are drawn.

2- Mathematical analysis.

The full-vectorial wave equations based on electric fields can be derived from the Maxwell's equations [16]:

$$\nabla \times E = -j\omega\mu_o H \quad (1)$$

$$\nabla \times H = j\omega n^2 \varepsilon_o E \quad (2)$$

$$\nabla \cdot \left(n^2 E\right) = 0 \quad (3)$$

$$\nabla \cdot (H) = 0 \quad (4)$$

First by taking the curl of Eq. (1) and substituting using equation Eq. (2):

$$\nabla \times \nabla \times E - n^2 k^2 E = 0 \quad (5)$$

where $k=\omega/c$ is the free space wave number and $c = 1/\sqrt{\mu_o \varepsilon_o}$ is the velocity of light in free space.

By using the vector identity

$$\nabla \times \nabla \times = \nabla(\nabla .) - \nabla^2 \quad (6)$$

Eq. (5) becomes

$$\nabla^2 E + n^2 k^2 E = \nabla(\nabla \cdot E) \quad (7)$$

If the transverse components of an electromagnetic field are known, then the longitudinal component may be readily obtained by applying Eq. (3). Therefore, the transverse components are sufficient to describe the vectorial properties of the electromagnetic field. The transverse component of Eq. (7):

$$\nabla_t^2 E_t + n^2 k^2 E_t = \nabla_t \left(\nabla_t \cdot E_t + \frac{\partial E_z}{\partial z} \right) \quad (8)$$

and using Eq. (3):

$$\nabla_t \cdot \left(n^2 E_t\right) + \frac{\partial n^2}{\partial z} E_z + n^2 \frac{\partial E_z}{\partial z} = 0 \quad (9)$$

Since $n(x, y)$ is z-invariant, $\partial n^2 / \partial z = 0$, and so the longitudinal and transverse components are related by

$$\frac{\partial E_z}{\partial z} = -\frac{1}{n^2} \nabla_t \cdot \left(n^2 E_t\right) \quad (10)$$

Substituting Eq. (10) into Eq. (8), and using the transformation

$$E(x, y, z) = E(x, y) e^{-j\beta z} \quad (11)$$

one can derive the vectorial wave equation

$$\nabla_t^2 E_t + \left(n^2 k^2 - \beta^2\right) E_t = \nabla_t \left[\nabla_t \cdot E_t - \frac{1}{n^2} \nabla_t \cdot \left(n^2 E_t\right) \right] \quad (12)$$

Eq. (12) can be written in matrix form [16]

$$\begin{pmatrix} P_{xx} & P_{xy} \\ P_{yx} & P_{yy} \end{pmatrix} \begin{pmatrix} E_x \\ E_y \end{pmatrix} = \beta^2 \begin{pmatrix} E_x \\ E_y \end{pmatrix} \quad (13)$$

where the differential operators are defined as

$$P_{xx}E_x = \frac{\partial}{\partial x}\left[\frac{1}{n^2}\frac{\partial(n^2E_x)}{\partial x}\right] + \frac{\partial^2 E_x}{\partial y^2} + n^2k^2E_x \quad (14)$$

$$P_{xy}E_x = \frac{\partial^2 E_y}{\partial x^2} + \frac{\partial}{\partial y}\left[\frac{1}{n^2}\frac{\partial(n^2E_y)}{\partial y}\right] + n^2k^2E_x \quad (15)$$

$$P_{yx}E_y = \frac{\partial}{\partial x}\left[\frac{1}{n^2}\frac{\partial(n^2E_y)}{\partial y}\right] - \frac{\partial^2 E_y}{\partial x \partial y} \quad (16)$$

$$P_{yy}E_y = \frac{\partial}{\partial y}\left[\frac{1}{n^2}\frac{\partial(n^2E_x)}{\partial x}\right] - \frac{\partial^2 E_x}{\partial y \partial x} \quad (17)$$

Eq. (13) is a full-vector eigenvalue equation, which describes the modes of propagation for an integrated waveguide. The two coupled transverse field components E_x and E_y taken together are the eigenfunction, and the corresponding eigenvalue is β^2. The four remaining field components can be easily derived from these two transverse components by applying Maxwell's equations. The field is assumed zero at grid points immediately outside of the computation window.

In order to translate this partial differential equation into a set of finite difference equations, the second derivatives must be approximated in terms of the values of the fields at surrounding grid points. The subscripts N, S, E and W, were used to indicate the value of the field (or index profile) at grid-points immediately north, south, east and west of the point under consideration, P. Let one of the transverse field components denoted by $\varphi(x, y)$, then the partial differential equations can be approximated by:

$$\frac{\partial^2\phi}{\partial x^2}\Big|_P = \frac{1}{(\Delta x)^2}(\phi_W - 2\phi_P + \phi_E) \quad (18)$$

$$\frac{\partial\phi}{\partial x}\Big|_P = \frac{1}{2\Delta x}(\phi_E - \phi_W) \quad (19)$$

Similar finite difference approximations can be applied in the vertical direction:

$$\frac{\partial^2\phi}{\partial y^2}\Big|_P = \frac{1}{(\Delta y)^2}(\phi_S - 2\phi_P + \phi_N) \quad (20)$$

$$\frac{\partial\phi}{\partial y}\Big|_P = \frac{1}{2\Delta y}(\phi_N - \phi_S) \quad (21)$$

Where Δx and Δy are the gird spacing in x and y directions respectively.

One of the most straightforward techniques for deriving finite difference approximations is Lagrange interpolation [17]. The Lagrange interpolant is simply the lowest order polynomial which goes through all of the sample points. The derivatives can then be easily computed from the polynomial coefficients of the interpolating function. For example, to

approximate the second derivative of ϕ with respect to x at point P, $\partial^2\phi/\partial x^2|_P$, a quadratic equation was fitted to the three points ϕ_W, ϕ_P, and ϕ_W:

$$\phi(x) = \begin{cases} A_W + Bx + Cx^2 & \text{in cell W} \\ A_P + Bx + Cx^2 & \text{in cell P} \\ A_E + Bx + Cx^2 & \text{in cell E} \end{cases} \quad (22)$$

and the interpolating function passes through the three points e_{xW}, e_{xP} and e_{xE}:

$$e_{xW} = A_W - B\,\Delta x + C(\Delta x)^2 \quad (23)$$

$$e_{xP} = A_P \quad (24)$$

$$e_{xE} = A_E + B\,\Delta x + C(\Delta x)^2 \quad (25)$$

Moreover, with adding additional constraint that describes the continuity of $n^2 e_x$ at $x = \pm \Delta x/2$, one can get:

$$n^2_W\left\{A_W - \frac{1}{2}B\Delta x + \frac{1}{4}C\Delta x^2\right\} = n^2_P\left\{A_P - \frac{1}{2}B\Delta x + \frac{1}{4}C\Delta x^2\right\} \quad (26)$$

$$n^2_P\left\{A_P + \frac{1}{2}B\Delta x + \frac{1}{4}C\Delta x^2\right\} = n^2_E\left\{A_E + \frac{1}{2}B\Delta x + \frac{1}{4}C\Delta x^2\right\} \quad (27)$$

From Eq. (23) to Eq. (27) give five linear equations, which can be solved for the five unknown polynomial coefficients. (Actually, B and C are the only two coefficients of interest because they describe respectively the first and second derivatives of e_x) After some algebraic steps, one can get:

$$\frac{\partial\phi}{\partial x} = B = \frac{1}{\Delta x}\left\{\frac{-\left(n^2_W n^2_P + 3n^2_E n^2_W\right)e_{xW}}{n^4_P + 2n^2_E n^2_P + 2n^2_W n^2_P + 3n^2_E n^2_W} + \frac{3\left(n^2_E - n^2_W\right)n^2_P}{n^4_P + 2n^2_E n^2_P + 2n^2_W n^2_P + 3n^2_E n^2_W}e_{xP} + \frac{\left(n^2_E n^2_P + 3n^2_E n^2_W\right)}{n^4_P + 2n^2_E n^2_P + 2n^2_W n^2_P + 3n^2_E n^2_W}e_{xE}\right\} \quad (28)$$

$$\frac{\partial^2\phi}{\partial x^2} = 2C = \frac{1}{\Delta x^2}\left\{\frac{4\left(n^2_W n^2_P + n^2_E n^2_W\right)e_{xW}}{n^4_P + 2n^2_E n^2_P + 2n^2_W n^2_P + 3n^2_E n^2_W} + \frac{4\left(n^2_E n^2_P - n^2_W n^2_P + 2n^2_E n^2_W\right)n^2_P e_{xP}}{n^4_P + 2n^2_E n^2_P + 2n^2_W n^2_P + 3n^2_E n^2_W} + \frac{4\left(n^2_E n^2_P + n^2_E n^2_W\right)n^2_P}{n^4_P + 2n^2_E n^2_P + 2n^2_W n^2_P + 3n^2_E n^2_W}e_{xE}\right\} \quad (29)$$

Equations (18), (20) and (29), can be combined to yield the finite difference representation of the operator P_{xx}

0	$\frac{1}{(\Delta y)^2}$	0
$\frac{\alpha_W}{(\Delta x)^2}$	$n^2_P k^2 - \frac{2}{(\Delta y)^2} - \frac{2\alpha_P}{(\Delta x)^2}$	$\frac{\alpha_E}{(\Delta x)^2}$
0	$\frac{1}{(\Delta y)^2}$	0

(30)

Where α_W, α_P and α_E are, dimensionless ratios defined:

$$\alpha_W = \frac{4\left(n^2_W n^2_P + n^2_E n^2_W\right)}{n^4_P + 2n^2_E n^2_P + 2n^2_W n^2_P + 3n^2_E n^2_W} \quad (31)$$

$$\alpha_P = \frac{2\left(n^4_P - n^2_E n^2_P + 2n^2_W n^2_P\right)}{n^4_P + 2n^2_E n^2_P + 2n^2_W n^2_P + 3n^2_E n^2_W} \quad (32)$$

$$\alpha_E = \frac{4\left(n^2_E n^2_P + n^2_E n^2_W\right)}{n^4_P + 2n^2_E n^2_P + 2n^2_W n^2_P + 3n^2_E n^2_W} \quad (33)$$

A similar treatment can be done to have the other operators P_{yy}, P_{xx} and P_{yx}

As described above, the finite difference method essentially translates a partial differential eigenvalue equation into a conventional matrix eigenvalue equation. The partial differential operators have been replaced by large sparse matrices, and the eigenfunctions have been replaced by long vectors representing a sampling of the eigenfunctions at discrete grid-points. Once this matrix equation was set up, one must solve for the eigenvalues and eigenvectors. Naturally, since the matrix is of dimension $M = n_x n_y$ (where n_x and n_y is the number of girds in x and y directions respectively), there should be M eigenpairs. There are many routines available for computing a few selected eigenvalues of large sparse matrices. The most common technique is the shifted inverse power method [18]. Unfortunately, this technique proves to be relatively slow and it is only capable of computing one eigenfunction at a time. One of the most promising algorithms is the implicitly restarted Arnoldi method [19]. This method allows one to simultaneously compute a few of the largest eigenvalues of the sparse matrix. For this work, we used the built-in Matlab function eigs, which implements the Arnoldi method.

Once the propagation constant is obtained, the chromatic dispersion D of a PCF can then be calculated from the n_{eff} values versus the wavelength using

$$D = -\frac{\lambda}{c}\frac{d^2 n_{eff}}{d\lambda^2} \quad (34)$$

The material dispersion given by Sellmeier's formula [20] is directly included in the calculation.

The effective mode area can also be calculated using [21]:

$$A_{eff} = \frac{\left(\int_1^{ny}\int_1^{nx}|E(x,y)|^2\,dxdy\right)^2}{\int_1^{ny}\int_1^{nx}|E(x,y)|^4\,dxdy} \quad (35)$$

3-Validation and numerical results

A program implementing the FV-FDM method has been made. In order to check the numerical precision of the program, standard rib waveguide structure whose cross section is shown in Fig.1 will be analyzed. The rib width, W is 3.0 μm, the rib height, H, and the outer slab depth, D, are such that H+D =1.0 μm, and the operating wavelength is 1.15 μm. The refractive indices of the guiding, n_g, and substrate, n_s, regions are 3.44 and 3.4, respectively.

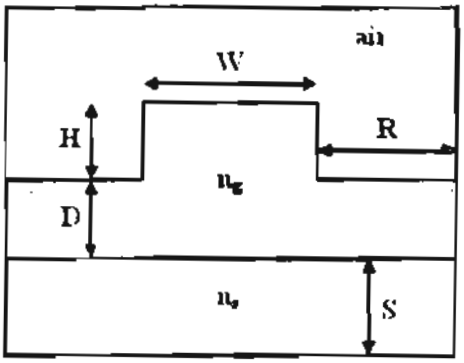

Fig.1. Schematic diagram of the rib waveguide structure.

Table 1 shows the values of the effective index of the fundamental mode as the outer slab depth, D, varies from 0 to 0.9 μm. These results were obtained by using the FV-FDM and other vectorial formulations including the vector finite-element method (VFEM) with the results from the Aitken extrapolation [22], the iterative vector finite-difference method with the transparent boundary condition (IVFDM) [23], the semivectorial finite-difference method (SVFDM) [24], the VFEM with higher order mixed-interpolation-type elements (Edge-FEM) [25] and full vectorial finite element based beam propagation method (IDVFEBPM) [26]. As may be seen from the table, there is good agreement between the results of the FV-FDM program and other formulations.

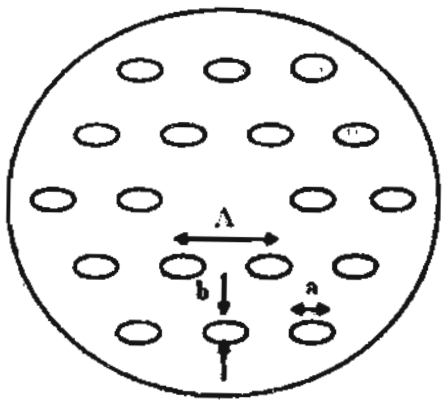

Fig.2. Cross section of a PCF of two rings of 18 elliptical air holes.

D(μm)	VFEM	VFDM	SV-FDM	Edge-FEM	IDVFEBPM	FV-FDM
0.1	3.41220	3.41211	3.41200	3.41209	3.41213	3.41222
0.2	3.41235	3.41226	3.41217	3.41224	3.41229	3.41234
0.3	3.41255	3.41247	3.41240	3.41247	3.41250	3.41252
0.4	3.41285	3.41275	3.41271	3.41278	3.41279	3.41279
0.5	3.41315	3.41311	3.41310	3.41312	3.41314	3.41314
0.6	3.41365	3.41355	3.41358	3.41358	3.41358	3.41360
0.7	3.41410	3.41408	3.41415	3.41414	3.41410	3.41415
0.8	3.41475	3.41472	3.41484	3.41480	3.41473	3.41480
0.9	3.41560	-	3.41568	3.41568	3.41553	3.41554

Table1: Effective index for the rib waveguide, shown in Fig.1, for Different values of D, D + H = 1 μm , S = 1.1 μm and W = 3 μm at λ = 1.15 μm.
Column 2 (VFEM [22]). Column 3 (IVFDM [23]). Column 4 (SV-FDM [24]). Column 5 (Edge-FEM [25]). Column 6: (IDVFEBPM [26]). Column 7: Present work

Then the FV-FDM program has been used for performing modal solution for different PCFs structures. Fig. 2 shows a schematic diagram of the PCF, consisting of two rings of arrays of elliptical air holes with a and b are the semiaxes of the elliptic holes (the "radii" in each direction.). They are arranged with hole pitch Λ in a silica background whose index of refraction taken as 1.45 at a wavelength of 1.55 mm.

For two rings of 18 air holes with Λ=2 μm, the effect of varying a or b on the effective index, the dispersion and the effective mode area was tested. First a was kept constant at 0.6 μm while varying b, then keeping b constant at 0.6 μm while varying a. The computing window size is 12 μm ×12 μm. For a 120×120-grid division, the computation time is 20.531 seconds for one wavelength using a Pentium IV 1.6-GHz, 256 MB Ram personal computer. Fig.3.a, Fig.3.b and Fig.3.c show that, the effective index, the dispersion and the effective mode area of the fundamental mode obtained from the two cases are approximately identical. It may be noted that, the effective index and the effective mode area for PCF with circular holes (a=b) are less than that for PCF with elliptical holes while the

dispersion is greater. It can also be noted that, with increasing the ratio (a/b) if (a>b) or increasing the ratio (b/a) if (b>a), the effective index and the effective mode area increase while the dispersion decreases. The dispersion curves become more flat and the zero dispersion wavelength is shifted to long wavelength region with increasing the above ratios. So one can reach the zero dispersion at the desired wavelength by controlling a and b values. Therefore, if PCF with circular holes is exposed to external pressure and the holes are deformed into elliptical ones, one can expect the exposed pressure from the behavior of the effective index, the dispersion or the effective mode area.

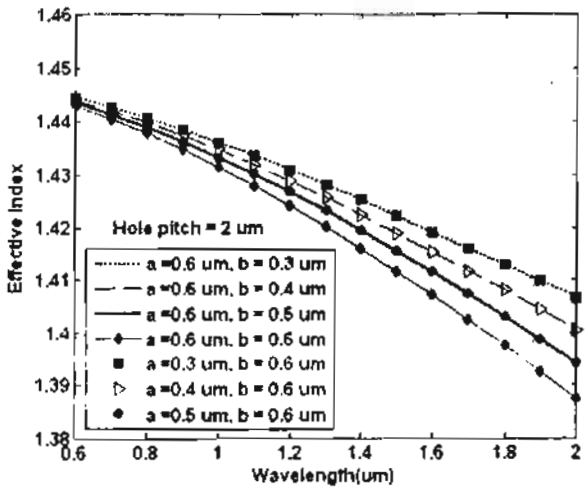

Fig.3.a Variation of effective index of the fundamental mode of two-ring PCF with elliptical holes with wavelength with a and b as parameters at Λ= 2 μm

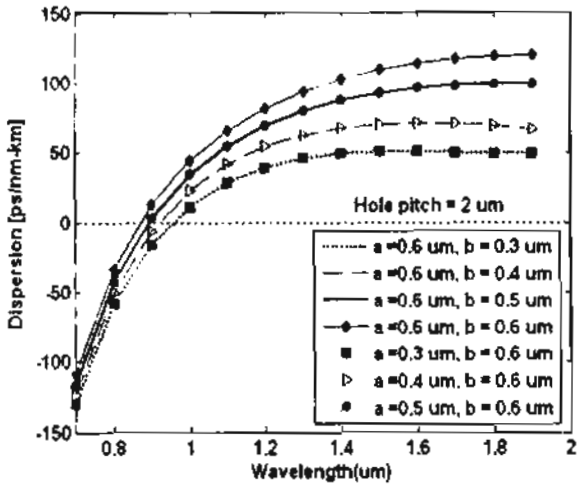

Fig.3.b Variation of dispersion of the fundamental mode of two-ring PCF with elliptical holes with wavelength with a and b as parameters at Λ= 2 μm

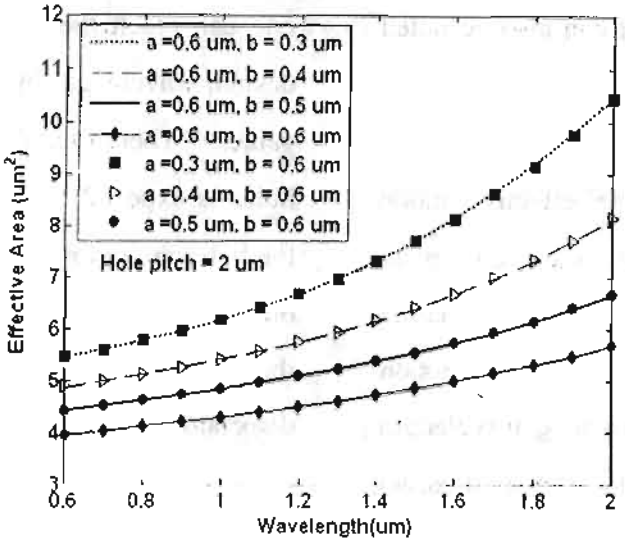

Fig.3.c Variation of effective mode area of the fundamental mode of two-ring PCF with elliptical holes with wavelength with a and b as parameters at Λ= 2 μm

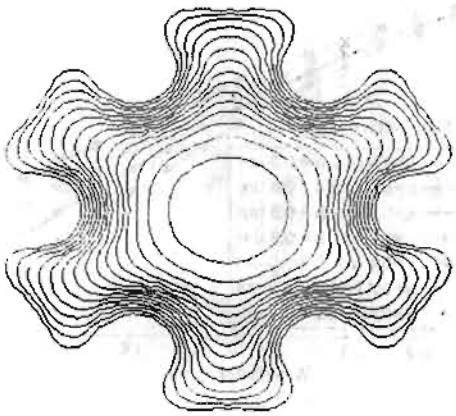

Fig.4.a The field distribution (E_x) of the fundamental mode of two-ring PCF with Λ= 2 μm and a=b= 0.6 μm at λ= 0.8 μm

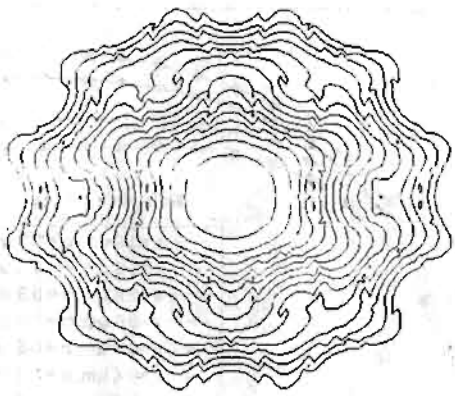

Fig.4.b The field distribution (E_x) of the fundamental mode of two-ring PCF with Λ= 2 μm and a=b= 0.6 μm at λ= 1.8 μm

Fig.4.a and Fig.4.b show that the mode becomes less confined to the core region with increasing the wavelength, so the effective index decreases with increasing the wavelength while the effective mode area increases as shown in Fig.3.a and Fig.3.c respectively.

Then we considered the inner ring of the PCF has circular holes while the other ring has elliptical holes. The hole radius in the first ring was kept constant at 0.6 μm while varying a and b of the elliptical holes in the outer ring. If b increases while a is still constant, it is noted that there is no noticeable change in the effective index as shown in Fig.5.a. However, at long wavelength the dispersion increases while the effective mode area decreases as shown in Fig.5.b and Fig.5.c The zero dispersion wavelength is not affected in this case. This ensures that the geometry of the holes in the first ring has the great effect on the effective index of the fundamental mode. So if an external pressure is exposed to PCF with circular holes and it deforms the holes in the second ring only into elliptic ones, then this PCF can be used as pressure sensor only at long wavelength. One can predict the pressure from the dispersion and the effective mode area curves only at long wavelength and no information can be expected in this case from the effective index curves. The above simulation was repeated with varying a and b of the elliptical holes of the outer ring but having the same area of the circular holes (that means $a \times b = (0.6)^2$). No significant change was obtained in the effective index, dispersion or in the effective mode area when changing the parameters of the outer elliptical holes when they have the same area of the first circular holes.

Keeping the area of the low index core constant, comparison between low index circular and elliptical core was made. Consider the holes of the two rings of the PCF are elliptical (a=0.6 μm, b=0.4 μm) and low index core with $a' \times b' = (0.3)^2$ μm^2. Fig.6.a shows that there is also slight difference between the effective index of the low index circular and elliptical core when they have the same area. The dispersion and the effective mode area are shown in Fig.6.b, Fig.6.c respectively. The same results are obtained when the holes of the two rings

of the PCF are circular. It may be noted from dispersion curves at a'= 0.4 μm and b'= 0.225 μm that the dispersion curve is approximately flat in the wavelength range from 1.3 μm to 1.8 μm with dispersion 0±1.288 ps/nm.km. So zero and flat dispersion can be achieved by changing the geometrical parameters of the elliptical low index core PCF with elliptical holes

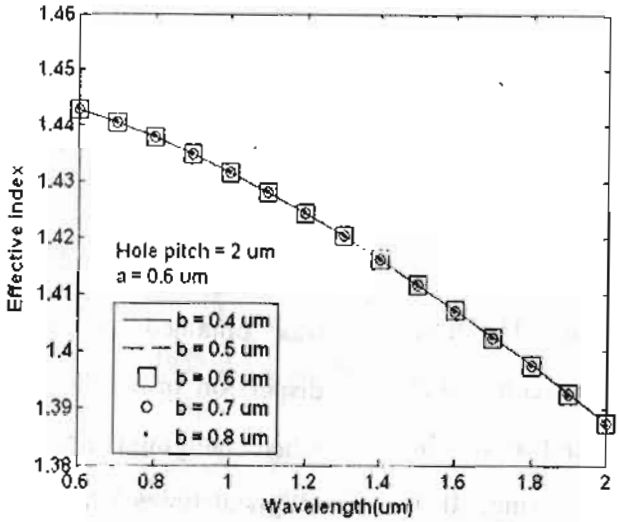

Fig.5.a Variation of effective index of the fundamental mode of two-ring PCF with wavelength with b of the elliptic holes in the second ring as a parameter while keeping (a = 0.6 μm), circular holes radius in the first ring (r = 0.6 μm) and (Λ =2 μm) constants

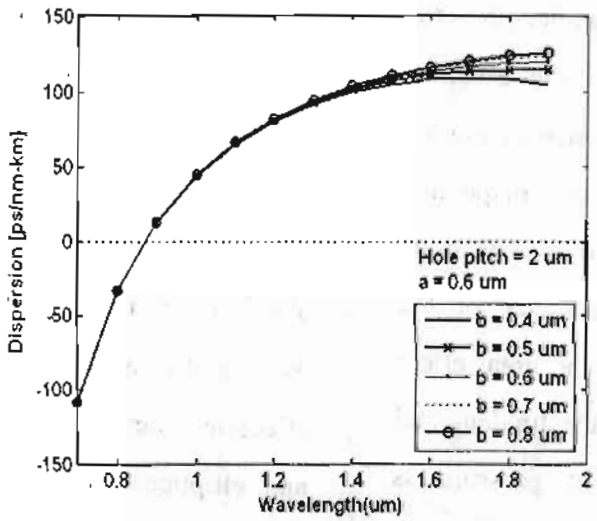

Fig.5.b Variation of dispersion of the fundamental mode of two-ring PCF with wavelength with b of the elliptic holes in the second ring as a parameter while keeping (a = 0.6 μm), circular holes radius in the first ring (r = 0.6 μm) and (Λ =2 μm) constants

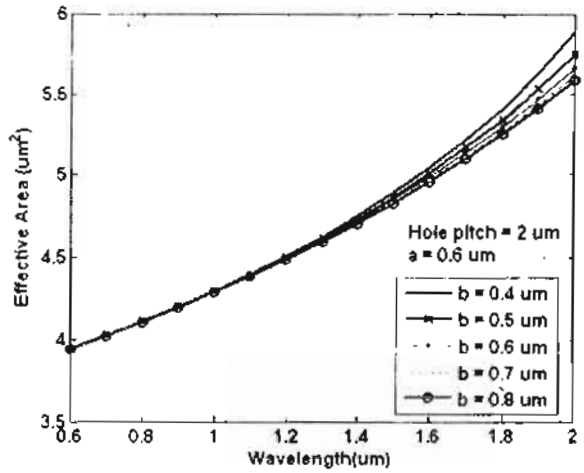

Fig.5.c Variation of effective area of the fundamental mode of two-ring PCF with wavelength with b of the elliptic holes in the second ring as a parameter while keeping (a = 0.6 μm), circular holes radius in the first ring (r = 0.6 μm) and (Λ =2 μm) constants

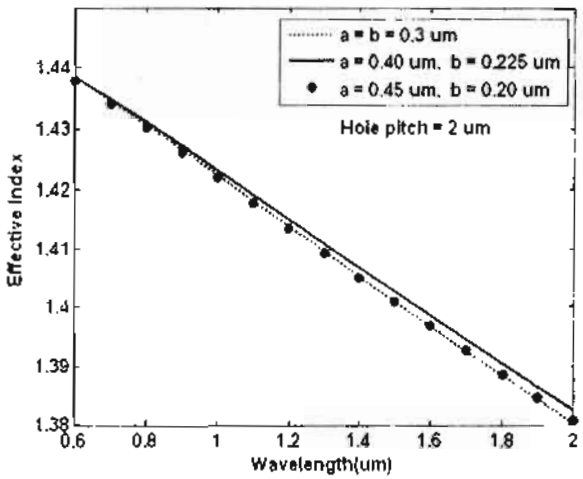

Fig.6.a Variation of effective index of the fundamental mode with wavelength with a and b of the central hole as parameters but having the same elliptical central hole area. The surrounding holes are elliptical.

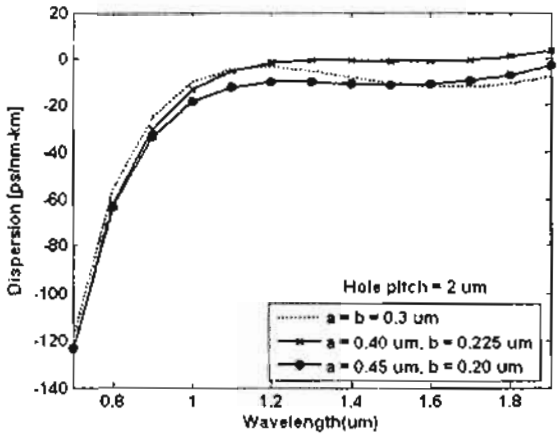

Fig.6.b Variation of dispersion of the fundamental mode with wavelength with a and b of the central hole as parameters but having the same elliptical central hole area. The surrounding holes are elliptical.

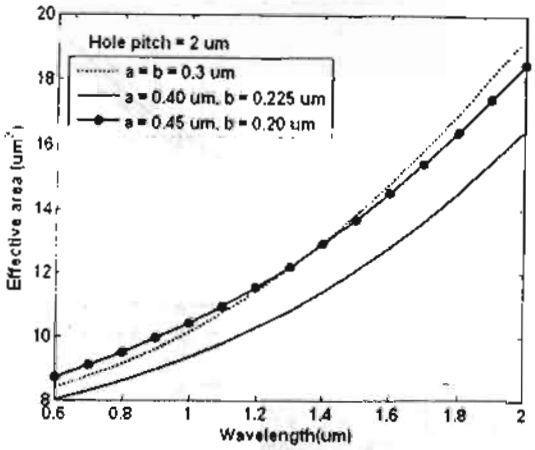

Fig.6.c Variation of effective area of the fundamental mode with wavelength with a and b of the central hole as parameters but having the same elliptical central hole area. The surrounding holes are elliptical.

4-Conclusion

The FV-FDM has been applied to perform modal analysis of different PCFs structures with circular and elliptical holes. The effects of the geometrical parameters of the holes on the modal properties, such as the effective index, dispersion and the effective mode area are studied. The possibility of tailoring the PCF structure, to achieve zero dispersion at the desired wavelength has been also studied. Flat dispersion with D= 0±1.288 ps/nm.km over the wavelength range from 1.3 μm to 1.8 μm has been reported. So with further optimization of the structure parameters, these dispersions can be reduced still further. If an external pressure is exposed to PCF with circular holes and all the holes are deformed into elliptical ones, this PCF can be used as pressure sensor. Pressure sensing can be obtained from effective index, dispersion and effective mode area curves. However, if the deformation occurs in the outer holes only, the pressure sensing can be obtained only from dispersion and the effective mode area curves at longer wavelength. No information can be expected in this case from the effective index curves.

5- References

[1] J.Broeng, D.Mogilevstev, S.E.Barkou, and A.Bjarklev, Photonic crystal fibers: A new class of optical waveguides, Opt. Fiber Technol. 5 (1999) 305-330.

[2] T.A.Birks, J.C.Knight, B.J.Mangan, and P.S.J.Russell, Photonic crystal fibers: An endless variety, IEICE Trans. Electronm E 84-C (2001) 585-592.

[3] T.A.Birks, J.C.Knight, and P.S.J.Russell, Endlessly single-mode photonic crystal fibre, Opt. Lett. 22 (1997) 961–963.

[4] J.C.Knight, T.A.Birks, R.F.Cregan, P.S.J.Russell and J.P.de Sandro, Large mode area photonic crystal fiber, Electron. Lett. 34 (1998) 1347–1348.

[5] M.J.Gander, R.McBride, J.D.C.Jones, D.Mogilevtsev, T.A.Birks, J.C.Knight, and P.St.J. Russell, Experimental measurement of group velocity in photonic crystal fiber, Electron. Lett. 35 (1998) 63–64.

[6] J.T.Lizier and G.E.Town, Splice losses in holey optical fibers, IEEE Photonics Technol. Lett., 13 (2001) 794–796.

[7] C.P.Yu, and H.C.Chang, Applications of the finite difference mode solution method to photonic crystal structures, Opt. Quantum Electron. 36 (2004) 145–163.

[8] A.Cucinotta, S.Selleri, L.Vincetti and M.Zoboli, Holey fiber analysis through the finite element method, IEEE Photonics Technol. Lett. 14 (2002) 1530–1532.

[9] M.Koshiba and K.Saitoh, Polarization-dependent confinement losses in actual holey fibers, IEEE Photonics Technol. Lett. 15 (2003) 691–693.

[10] M.J.Robertson, S.Ritchie and P.Dayan, Semiconductor waveguides: analysis of optical propagation in single rib structures and directional couplers, Inst. Elec. Eng. Proc.J. 132 (1985) 336–342.

[11] M.S.Stern, semivectorial polarized finite difference method for optical waveguides with arbitrary index profiles, Inst. Elec. Eng. Proc.J. 135 (1988) 56–63.

[12] C.Vassallo. Improvement of finite difference methods for step-index optical waveguides. Inst. Elec. Eng. Proc.J. 139 (1992) 137-142 .

[13] K. Bierwirth. N.Schulz. and F.Arndt. Finite-difference analysis of rectangular dielectric waveguides by a new finite difference method. J. Lightwave Technol. 34 (1986) 1104 1113.

[14] P.Lusse, P.Stuwe, J.Schule and H.G.Unger. Analysis of vectorial mode fields in optical waveguides by a new finite difference method. J. Lightwave Technol. 12 (1994) 487–494.

[15] G.L.Xu. W.P.Huang. M.S.Stern and S.K.Chaudhuri. Full-vectorial mode calculations by finite difference method . IEE Proc.-Optoelectron. 141 (1994) 281-286.

[16] A.S.Sudbo. Film Mode Matching: a Versatile Numerical Method for Vector Mode Field Calculations in Dielectric Waveguides. Pure and Applied Optics 2 (1993) 211-233.

[17] J. Peraire. Finite Difference Discretization of Elliptic Equations. 1999. Course notes from 16.920 (Numerical Methods for Partial Differential Equations).

[18] M.S.Stern. Semivectorial polarised finite difference method for optical waveguides with arbitrary index profiles. IEE Proc. J 135 (1988) 56-63

[19] D.C.Sorensen, Implicit Application of Polynomial Filters in a k-step Arnoldi method. SIAM J. Matrix Analysis and Applications. 13(1) (1992) 357 – 385

[20] G.P.Agrawal. Fiber-optic communication systems. (John Wiley & Sons. 1997. 2nd Edn.). 41–42

[21] K.Saitoh and M.Koshiba, Chromatic dispersion control in photonic crystal fibers: application to ultra-flattened dispersion. Opt. Express. 11 (2003) 843–852.

[22] B.M.A.Rahman and J.B.Davies. Vector-H finite element solution of GaAs/GaAlAs rib waveguides. Proc. Inst.

Elect. Eng. Optoelectronics 132 (1985) 349–353.

[23] G.R.Hadley and R.E.Smith. Full-vector waveguide modeling using an iterative finite-difference method with transparent boundary conditions, J. Lightwave Technol. 13 (1995) 465–469.

[24] M.S.Stern, Semivectorial polarized finite difference method for optical waveguides with arbitrary index profiles. Proc. Inst. Elect. Eng. Optoelectronics. 135 (1988) 56 -63.

[25] M.Koshiba, S.Maruyama and K.Hirayama. A vector finite element method with the high-order mixed-interpolation-type triangular elements for optical waveguiding problems. J.Lightwave Technol.. 12 (1994) 495–502.

[26] S.S.A.Obayya. B.M.A.Rahman. K.T.V.Grattan and H.A.El-Mikati. Full vectorial finite-element-based imaginary distance beam propagation solution of complex modes in optical waveguides, J. Lightwave Technol. 20 (2002) 1054–1060.